

THE INTERNATIONAL JOURNAL OF SCIENCE & TECHNOLEDGE

Measurement of Non Perfused Size (Area) of Spect Images Using ImageJ Software

Hayatu Mohammed

Medical Physicist, Department of Radiology, University of Maiduguri Teaching Hospital,
Maiduguri, Borno State, Nigeria

Medical Physicist, School of Physics, Universiti Sains Malaysia, Pulau Pinang, Malaysia

Dr. Norlaili Ahmad Kabir

Senior Lecturer, School of Physics, Universiti Sains Malaysia, (USM), Pulau Pinang, Malaysia

Fahad Usman

Lecturer, Department of Physics, Alqalam University, Katsina State, Nigeria
School of Physics, Universiti Sains Malaysia, Pulau Pinang, Malaysia

Khairul Jafar Nizam

Nuclear Medicine Technician, Nuclear Medicine Unit, Advance Medical and Dental Institute USM,
Bertam Pinang, Malaysia

Alsaya Mohannad

Ph.D. Student, School of Physics, Universiti Sains Malaysia, Pulau Pinang, Malaysia

Mannawi Nasiru Isa

Lecturer, Department of Physics, Alqalam University, Katsina State, Nigeria

Abstract:

Computer-aided diagnosis (CAD) using Image J software has been used to quantify myocardial infarct (MI) area. The study was designed to develop an algorithm for thresholding of myocardial perfusion SPECT image, and estimate an area with possible myocardial infarction from region with normal perfusion. The objective of this paper is to determine the accuracy of ImageJ algorithm for quantification of myocardial infarct area using SPECT images.

A phantom consists of a large container to mimic the human body. With a small cylindrical container inserted in the large container to simulate the heart, inside the small cylindrical container, a silicon rubber and some defects (40 mm² each) were placed to mimic the heart Myocardium and perfusion defects. A ^{99m}Tc – tagged (0.6 ml) radioisotope was mixed with water in the large container for background solution, the small cylindrical container was also filled with water and mixed with ^{99m}Tc – tagged (0.25 ml) radioisotopes, SPECT images were acquired and reconstructed with FBP technique using the Butterworth filter cut off frequency 0.4cm⁻¹ and order of 10. MI was quantified before and after thresholding using Image J software.

Overestimation of defect area was observed from the image without thresholding, with estimated mean area and standard deviation of about 273.93mm² ± 28.088, in comparison with the thresholded image with 38.09mm² ± 0.657. The thresholded image almost approximate the actual infarct size. At 0 cm position, the mean area and standard deviation were 33.51 mm² ± 0.436, and at the 10 cm position is about 38.09mm² ± 0.657. At 10 cm position, the defects areas almost approximate the actual infarcts size. We compare the mean area of the two positions using the paired t-test, a p-value of <0.001 was estimated, which indicates a strong statistical significance difference. The results indicate that, thresholding using ImageJ software not only aid in accurate infarcts quantitation, it also increases the signal to noise ratio, which enhances the contrast of the region of interest.

Keywords: Image J, Computer-aided diagnosis, SPECT, Myocardial infarction, Phantom, thresholding, Filtered back projection

1. Introduction

Nuclear Medicine imaging is fast growing, but the challenges of interpretation for efficient diagnosis have been its setbacks over the years. Due to these challenges, Clinicians do not make optimal use of the information acquired by an imaging device (Lusted, 1960). The imperfections of the human eye-brain system, insufficient training and experience, challenges such as lack of concentration, stress, distraction and environment may all add-up to suboptimal use of available information (Kundel & Revesz, 1976). Image

processing techniques can be employed to medical images with the intent to address some of these challenges. Medical image processing attempts to enhance the image presented to the readers in such a manner that abnormalities are enhanced for the reader to appreciate it. However, image processing alone cannot completely address these challenges such as inexperience and lack of concentration. Computer-aided diagnosis (CAD) systems applied to medical images suffice image processing, that is to say, they may provide specific lesion location information and/or other diagnostic analysis to assist clinicians.

The main objectives of computer-aided diagnostic system are to systematically identify areas in an image that may bring to light specific aberration and inform the expert to these locations during image interpretation. In addition, CAD system assists the clinician to exactly know the extent and progression of disease, in other to quantify and assess disease type, severity and stage of the disease (Doi, 2007).

The main objective of this paper is to determine the accuracy of ImageJ algorithm for quantification of myocardial infarct area, using SPECT images. ImageJ software have demonstrated to be valuable and reliable software for image analysis, is a public domain Java image processing and analysis program inspired by National Institutes of Health (NIH), United States of America which is freely available and operates on a range of platforms such as Windows, Mac, and Linux for image processing (Collins, 2007). It can calculate area and pixel value statistics of user-defined selections. It can measure distances and angles. It can create density histograms and line profile plots. It supports standard image processing functions such as contrast manipulation, sharpening, smoothing, edge detection and Median filtering (Pedersen, Steinkuhler, Wesser, & Rotilio, 2011). ImageJ software can read different file formats (without the need of third-party plugins), it opens the following formats: TIFF, GIF, JPEG, PNG, DICOM, BMP, PGM and FITS. (Hartig, 2013).

With ImageJ software, thresholding is one of the unique methods in separating pixels which fall in between a desired range of intensity values from those which do not, (also known as 'segmentation'). In the ideal world, the pixel intensity values of the areas you are interested in will be a unique subsection of the image; this will assist in distinguishing benign region from normal. The variability of human internal organs in density is what is exploited in general Radio-diagnostic, including nuclear medicine, this unevenness in tissue density will result in different absorption characteristics of the tissue to radiation, and this will lead different pixel intensities in different region inside our body structure. Selecting a particular pixel intensities and thresholding will lead to the subtraction of some range of pixel intensity intensities while enhancing and analyzing the selected Region of Interest (ROI). Quantification of ROI is also possible to ascertain or estimate the area of deficit in terms myocardial infarction.

Single photon emission computed tomography (SPECT) perfusion imaging has been considered a reference method for non-invasive estimation of infarct size in man. Computer aided diagnostic has evolved as an accurate tool to quantify infarct size. SPECT images have challenges of inherent noise due to attenuation and scattering of radiation, these challenges affect the interpretation of nuclear medicine images, with the development of hybrid imaging systems, i.e., SPECT/CT, apart from anatomical mapping, CT also takes care of the attenuation, which reduces the noises that may affect image quality.

The gamma camera, invented by Anger in the 1950, is a device for imaging the spatial distribution of a radionuclide in an object. The technique can be used for obtaining planar images as well as for tomographic imaging, where a number of projections in different angels of the object are collected and a three dimensional volume is obtained through either filtered back projection or an iterative method such as Maximum Likelihood Expectation Maximization (MLEM) or Ordered Subsets Expectation Maximization (OSEM). The iterative methods may also incorporate compensations for attenuation, scattering and collimator response as a part of the reconstruction. The tomographic use of the camera is often referred to as Single Photon Emission Computed Tomography, or SPECT. Myocardial perfusion imaging (MPI) is a generally used diagnostic method for handling of patients with suspected or known ischemic heart disease(Hachamovitch et al., 1996; Underwood et al., 2004). In Nuclear medicine, analysis of MPI relies on the knowledge of the clinicians, and is subject to inter and intra-observer variability(Lindahl, Lanke, Lundin, Palmer, & Edenbrandt, 1999).

1.1. Basic Principles of Cardiac SPECT Imaging

1.1.1. Myocardium Data Acquisition

SPECT provides three-dimensional images that facilitate both a visual and a quantitative evaluation of the cardiac radionuclide distribution and of the surrounding tissues by removing superimposed activity from surrounding tissues(DePuey & Rozanski, 1995).

The administered radioisotope in the patient's body emits single gamma ray photons that are recorded through a gamma camera mounted on a gantry in numerous projections around the patient. Both contour and elliptical orbits can be used. The projection acquisition may be performed in three different ways: step-and-shoot, continuous, and continuous step-and-shoot. The method mostly used is the step-and-shoot method. For a given orbit, the camera stops at predefined angular positions and acquires a projection for predefined time durations. An arc of 180 degrees is usually covered, that is, 45 degrees right anterior oblique to left posterior oblique (RAO-LPO) (DePuey & Rozanski, 1995). Equal times are used to achieve the same count statistics. Another parameter that greatly affects the image quality (sensitivity and resolution) is the choice of the collimator. This is determined mainly by the tracer activity. When ^{201}Tl is being used a low-energy general purpose collimator is traditionally chosen. For ^{99}Tc -labeled agents high resolution collimators are recommended, whereas for ^{111}In and ^{123}I MIBG (metaiodobenzyl guanidine) medium energy collimators are usually used (DePuey & Rozanski, 1995)

Other important parameters that are to be taken into account during acquisition are the projection matrix size, the number of angles, and the time per view. For the projection matrix, a common rule of thumb is that at least three pixels should be used to image a structure for each full width at half maximum (FWHM) of the response profile. For the number of angles the time per view determines the statistical content of the projected image. The interrelationship of these parameters is quite complicated. In most cardiac SPECT

protocols, a 180° camera rotation with 64×64 matrix size is recommended (Germano, 2001). The 2D projection-images are first corrected for non-uniformities and then mathematical algorithms are used to reconstruct 3-D matrices of selected planes from the 2-D projection data.

1.2. Myocardium Image Reconstruction Techniques

The purpose of reconstruction algorithms is to calculate an accurate 3-D radioactivity distribution from the acquired projections. There are two methods to reconstruct SPECT images, either by filter back projection (FBP) analytical technique or iteratively, by algebraic methods.

1.2.1. Filtered Back Projection Method (FBP)

Filtered back projection is an analytical method that is still the most widely used in clinical SPECT because of its simplicity, speed, and computational efficiency. FBP consists of two steps: Filtering of data and back projection of the filtered data (S. Cherry, Sorenson, & Phelps, 2003). In 2-D acquisition, each row of projections represents the sum of all counts along a straight line through the depth of the object being imaged. Back projection technique redistributes the number of counts at each particular point back along a line from which they were originally detected. This process is repeated for all pixels and all angles. A limited number of projection sets can result in the formation of the star artifact and in blurring of the image. To eliminate this problem, the projections are filtered before being back projected onto the image matrix. It has to be noticed that the back projection process has taken place in spatial domain while data filtration is done in the frequency domain. While the analytic approaches typically result in fast reconstruction algorithms, accuracy of the reconstructed images is limited by the approximations in the line-integral model on which the reconstruction formulae are based (Qi & Leahy, 2006). Cardiac SPECT reconstruction process may obtain attenuation corrections approximately, using a post processing step (Chang, 1978). Some reconstruction algorithms apply approximation formulas to the projection data for attenuation correction. Lee –Tzuu (Chang, 1978) applied a simple, effective two-step procedure to the uncorrected image. For two-dimensional (2-D) SPECT with Parallel or fan beam collimators, 2-D filtered back projection (FBP) algorithms are routinely used for myocardium SPECT reconstruction.

1.2.2. Iterative Reconstruction Method

Iterative reconstruction starts with an initial estimate of the image (S. R. Cherry, Sorenson, & Phelps, 2012). Most of the times, the initial estimate is very simple, for example, a uniform activity distribution. Then a set of projection data is estimated from the initial estimate using a mathematical process called forward projection. The resulting projections are compared with the recorded projections and the differences between the two are used to update the estimated image. The iterative process is repeated until the differences between the calculated and measured data are smaller than a specified preselected value. For 3-D SPECT, the iterative reconstruction methods include algebraic methods like the algebraic reconstruction technique (ART) and statistical algorithms like MLEM or OSEM (Bruyant, 2002). The MLEM algorithm is a general approach to solving maximum likely hood problems through the introduction of a set of data which, if observed, would make the ML problem readily solvable. The algorithm then iterates between computing the mean of the complete data, given the observed data and the current estimate of the image, and maximizing the probability of the complete data over the image space. In the ordered subsets EM (OSEM) method the full set of views is divided in to subsets and the EM algorithm applied sequentially to each of these data sets in turn. This produces remarkable improvements in the initial convergence rate compared to MLEM (Qi & Leahy, 2006).

1.3. Image Filtering in Cardiac SPECT

Different filter types in SPECT imaging can produce different optimal results in processed images, such as star artifact reduction, noise suppression, or signal enhancement and restoration (Van Laere, Koole, Lemahieu, & Dierckx, 2001). The choice of filter for a given image processing task is generally a compromise between the extent of noise reduction, fine detail suppression, and contrast enhancement, as well as the spatial frequency pattern of the image data of interest. Filters that are commonly used on SPECT imaging are the Ramp filter, a high pass filter eliminating the star artifact and blurring, the Hanning filter, a low pass smoothing filter, the Hamming filter, also a low pass smoothing filter having a different amplitude at the cut off frequency, the Butterworth filter, which both smoothers noise and preserves the image resolution, the Parzen filter, the most smoothing low pass filter, and the Shepp-Logan filter, which is the least smoothing but has the highest resolution (Van Laere et al., 2001). Two enhancement filters also used in cardiac SPECT are the Metz filter, a function of modulation transfer function and the Wiener filter, which his based on the signal-to-noise ratio of the specific image. A more extensive presentation of all the mentioned filters can be found in “Filtering in SPECT Image reconstruction” (Lyra & Ploussi, 2011).

2. Materials and Methods

2.1. SPECT/CT

SPECT/CT General Electric (G.E) Discovery (NM/670) (Fig. 1) was used in this study, with a dual headed gamma-Camera and a low-dose 16-slice CT are mounted on the same Rotation platform. The CT operates at 120 KV-100 mA for purpose of attenuation correction and image registration, with a 0.5 sec rotational speed scanning time to acquire a 40 x 54 cm axial field of view, and the 20mm (4 x 5 mm) axial coverage per CT slice best matches SPECT resolution. The SPECT detector consists of 3/8 inch. NaI crystal,

electrically coupled with 59 Photo-Multiplier tubes (PMT), 1 Analog/Digital converter/PMT (1 ADC/PMT). Spatial resolution with Low Energy High Resolution (LEHR) Collimator of 7.4, with 24 rows maximum 16 slices/rotation time in spiral mode.



Figure 1: SPECT/CT BY G.E discovery model NM/CT670

2.2. Phantom

A polystyrene phantom was designed to mimic the myocardial perfusion study of a human, featuring an insert to simulate the human heart. The larger container/tank is made up of polystyrene whereas the insert is made up of silicon rubber enclose in a small cylindrical container made up of polystyrene, enclose in the small cylindrical container are defects attach to the silicon rubber to simulate perfusion defects, the defect were made from a soft plastic, 4 cm² (40 mm²) each. The phantom and the cardiac insert are designed to mimic myocardial perfusion study (Myocardial infarction) as shown in Fig. 2 below.

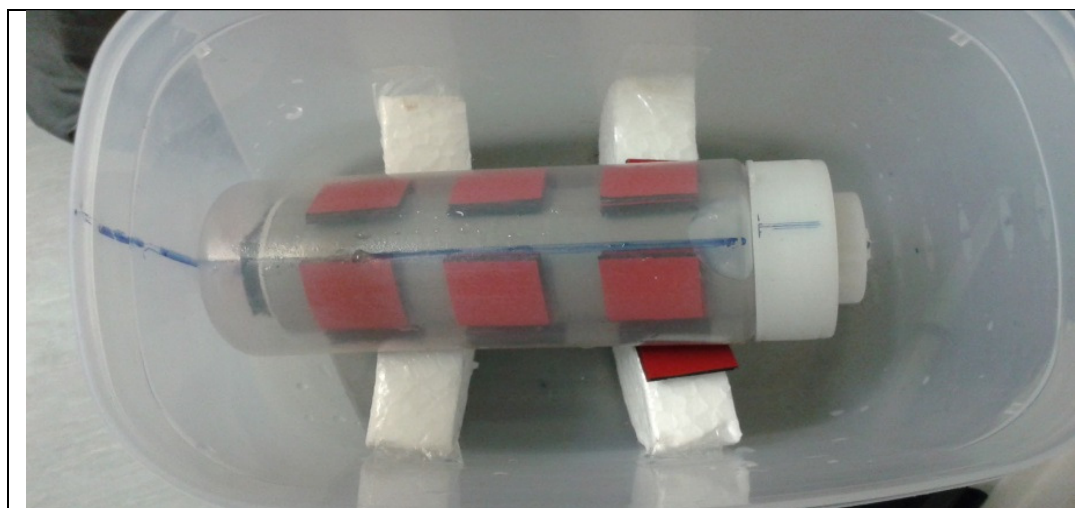


Figure 2: Polystyrene phantom to mimic myocardial perfusion studies (to study simulate myocardial infarction)

2.3. ImageJ Software

ImageJ software is application software built by Wayne Rasband, National Institutes of Health (NHI) United States of America which is freely available and operates on a range of platforms such as Windows, Mac, and Linux for image processing. The software can be employed to calculate various statistical parameters (i.e., mean, standard deviation, integrated density etc.) and can be used for quantification purpose, by thresholding and other selecting tools.

2.4. SPSS 21

SPSS 21.0 (SPSS Inc., Chicago, Illinois) is been used in this study, SPSS 21 is a comprehensive system for analyzing data. SPSS Statistics can take data from almost any type of file and use them to generate tabulated reports, charts, and plots of distributions and trends, descriptive statistics, and complex statistical analyses. SPSS Statistics makes statistical analysis more accessible for the beginner and more convenient for the experienced user. Simple menus and dialog box selections make it possible to perform Complex analyses without typing a single line of command syntax. The Data Editor offers a Simple and efficient spread sheet-like facility for entering data and browsing the working data file.

3. Methodology

3.1. SPECT Image Acquisition

Images were taken at an arc of 180 degrees, that is 45 degrees right anterior oblique to left posterior oblique (RAO-LPO). The imaging was performed using a hybrid double-head SPECT/CT camera [model GE Discovery dual headed SPECT/CT (NM/CT 670)] in A 90° geometry equipped with low-energy high resolution parallel-hole Collimators designed. The phantom was scan, and images were recorded over 180° in 256 x 256 matrices With an acquisition time of 20s per projection in 3° increments using the step and shoot mode, resulting in a total of 60 projections . The matrix used at 0 cm and 10 cm locations was 256 x 256. An energy window was centered on 140 keV ± 20% with a pixel size of 6.8 mm, planar image was the modality used. A stress perfusion imaging study was conducted (Fig 4), reconstructed By FBP (Filtered back projection) using the Butterworth filter cut off frequency 0.4 cm⁻¹ and order of 10 as a processing filter. Radiation transmission radionuclide was the mode of attenuation and scatter correction. Data acquired by GE Discovery dual headed SPECT/CT (NM/CT 670) and reconstructed in Nuclear Medicine unit, AMDI [Advanced Medical and dental institute (IPPT)], University of Science Malaysia (USM).



Figure 3: Phantom positioned at the center of the table while acquiring SPECT images

3.2. Image thresholding and Measurement of infarcts area using ImageJ Software

Thresholding works by separating pixels which fall within a desired range of intensity values from those which do not. The images reconstructed were selected from the vertical axis, five slices were selected from 0 cm, and 10 cm positions, the images are in DICOM format, in RGB (Red, Green and blue channel) color image, colors were assigned to perfused areas, less perfused areas and defected areas, example from fig 4, the white region was assigned to high perfused areas, yellow region were the sparsely perfused and blue region were the defected areas. To threshold the image in order to enhance defect area, RGB color image is converted in to 8 bits (gray scale), from the imageJ application tool bar, use Image> Type>8 bits. In 8 bit- grey scale, a pixel with an intensity of 0 is black, a pixel with a value of 255 is white, everything in between is a shade of grey. Inspecting the region of interest to check the average range of intensities in the region will assist during thresholding, in this study its around 128-pixel intensity or grey value. Segmentation (thresholding) involve the following, from the imageJ application tool bar, by using Image>Adjust>Threshold (or ctrl + shift+ t). The gate for the intensities measured can be adjusted by changing the minimum and maximum sliders, as shown from fig. 5. The values correspond to the pixel intensity value (0 = black and 255 = white in an 8 bit image). Adjust the values of the threshold until the region of interest is selected, adjusting the maximum and minimum sliders to 128, the defected area will be highlighted while the remaining pixel intensities will be subtracted from the image. Now, to measure the defected area, the average intensity and any other parameter of interest, be careful not to press “Apply” as this will make your image binary (i.e. black and white) and the red intensities information will be lost. To make measurements, set measurements and pick what you want in the set measurements window by ticking the box. Make sure that ‘Limit to Threshold’ is checked and ticked. If not all of the image will be measured. Scale need to be set, which before measuring the parameters, meaning to set the pixel values in to milli meter (mm), in this study its 6.8 pixel per mm. Make sure there is enough decimal places for accuracy. Once the measurements are set and the threshold is in place the SPECT image can be measured. This is done by going to Analyze >Measure, from the imageJ tool bar. The results of parameters selected will be displayed, and then you save it.

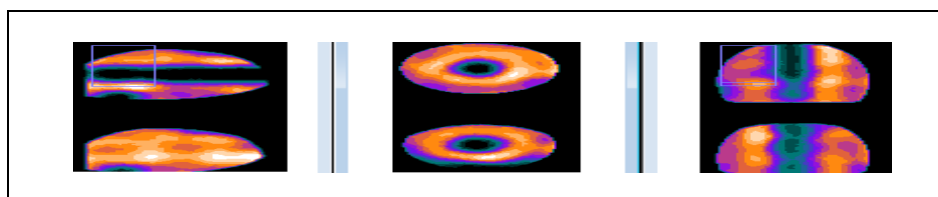


Figure 4: A stress perfusion imaging study, reconstructed by FBP using Butterworth filter

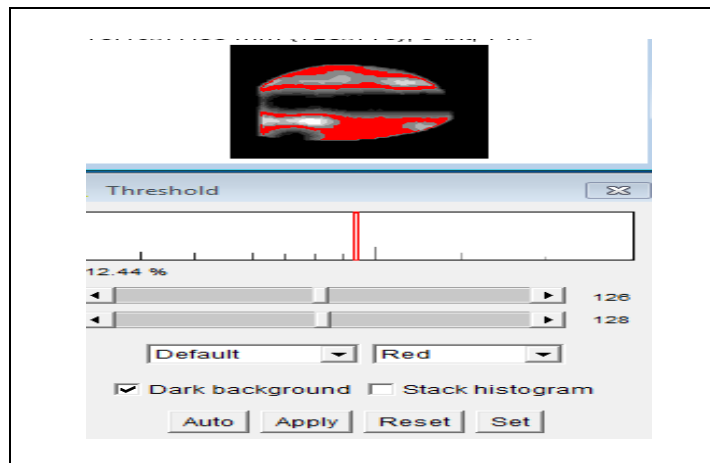


Figure 5: Example of thresholded image, the red color shade area is the defected area, whereas the white region is the highly perfused area

3.3. Statistical Analysis

Analyses were performed using SPSS 21 (SPSS Inc, Chicago, Illinois). Two tailed P values were used with $P \leq 0.05$ considered to indicate statistical significance. Or data are presented as mean \pm SD. One or two tailed (when appropriate) paired t-test were used to compare count activity between the images with or without thresholding. A P value < 0.05 was considered statistical significant.

4. Results and Discussions

4.1. Comparison between Measurement with Thresholding and without Thresholding

The table 1 below is the estimated area of defects, calculated using ImageJ software, before and after digital processes (thresholding).

With thresholding(mm ²)	No-thresholding/Raw data (mm ²)
37.327	313.365
37.543	273.659
38.214	266.263
38.495	235.316
38.906	281.055

Table1: estimated area from ImageJ of the thresholded and unthresholded data

Fig 6 below, are the five selected images that were digitally processed using ImageJ, the red color region is the defected area, whereas the white region are the highly perfused area.

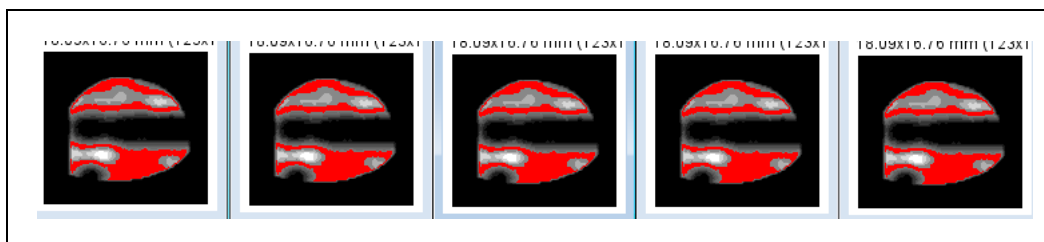


Figure 6: Thresholded image at 10 cm positioning of the phantom

Fig 7 below, are the same five selected images as in fig 6, the blue area in the image, is the defected area, the images also represents a raw data.

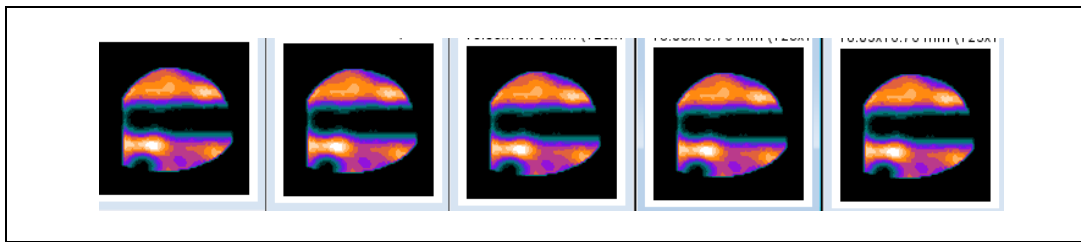


Figure 7: Unthresholded image (raw data) at 10 cm positioning of the phantom

Paired Samples Statistics					
		Mean	N	Std. Deviation	Std. Error Mean
Pair 1	mean1	38.09700	5	.656961	.293802
	mean2	273.93160	5	28.088174	12.561413

Table 2: mean area of the thresholded and unthresholded image calculated by SPSS 21

4.2. Discussion

The estimated area of perfusion defects in the reconstructed SPECT image is recorded in table 1, ImageJ was used to analyze and estimate the defects area for both thresholded and un-thresholded (raw data) image. Five different slices from the vertical-axis were chosen from the SPECT reconstructed images at 10 cm position.

The images were analyze before and after thresholding using ImageJ algorithm, the mean estimated area for the thresholded image were close to the actual size of the defects (40 mm^2), in comparison to the raw data, this could be due to image noises as a result scatter and attenuation of photons in the un-thresholded image.

From table 1, the estimated area of the slices selected varied a little; as an examining organ has certain dimensions, each slice along the axis of the gamma camera has different distance from the detector. Thus, each photon experiences different attenuation. These two phenomena usually lead to distortion of the measured activity concentration; this could be due to the slice thickness (1.70 mm) chosen during image reconstruction.

Another factor that could be responsible to the high noise in the un-thresholded image is the image reconstruction that was used. Filtered back projection (FBP) ignores physical phenomenon such as scatter and attenuation correction, which can cause significant image degradation. The quality of the myocardium SPECT images is degraded by several factors. The most important factors affecting image quality of myocardial perfusion SPECT are the statistical fluctuation in photon detection, the attenuation of photons and the scatter radiation. The reason for this is the fact that gamma rays have to travel some distance in a fluid media. This media attenuates and scattered the gamma radiation, the gammas being emitted actually get outside the body after traveling some distance in water. The further away the activity has to travel the greater the amount of attenuation occurs. Radiations are scattered in the phantom, and the scattered photons, depending on the energy and angle of scattering, may strike the detector. Scattering may occur in the detector itself, and also within or outside the FOV. Normally, most of these scattered photons fall outside the photopeak window and are rejected. However, a fraction whose photon energy falls within the photopeak window will be counted, but their (X, Y) positions remain uncertain causing degradation of the image resolution.

In addition to attenuation resulting in degrading the image quality which resulted in the increase of noise to the un-thresholded image, a significant fraction of the detected photons are scattered in the object. This is due to the finite energy resolution of the gamma camera, which results in imperfect energy based scatter rejection. The scatter to primary ratio (SPR) depends on the radionuclide, energy window, energy resolution, source depth and the size of the object. Scatter results in loss of contrast and quantitative accuracy. For an organ inside the patient body, SPR is in general greater for patients with large size than small size. Photons emitted from the organ have longer photon path in large patients than small patients, thus have higher probability to be scattered, and consequently SPR can be greater. The SPR increases approximately linearly with source depth, so the quantitative effects of scatter are larger for source positions near the centre of the object.

Radionuclide transmission sources was the method used for attenuation correction, some of the disadvantages that results in using such modality includes, the fact that the source decays and must be replaced. There are also limits on transmission count rates imposed by the gamma camera, resulting in relatively noisy transmission images. In addition, if the count rate due to the emission activity within the object is high, the transmission images can be degraded, resulting in inaccurate attenuation maps and consequently noisy image.

From table 2: SPSS 21 was used to calculate and compare the two means, i.e., mean area for the thresholded and un-thresholded image, the mean and standard deviation were $38.09 \pm 0.657 \text{ mm}^2$ (for thresholded) and $273.9 \pm 28.088 \text{ mm}^2$ (non thresholded).

The standard deviation (SD) is the measure of the signal to noise ratio, the higher the SD, the lower the signal to noise ratio, the thresholded image will have a better signal to noise ratio, because it has a lower standard deviation of ± 0.657 in comparison with the raw data with standard deviation of ± 28.088 which may result in better contrast for the thresholded image. The P-value is < 0.001 , which indicates a strong statistical significant difference between the two means.

4.2.1. Comparison between Estimated Areas at Two Different Positioning of the Phantom

Table 3 below is the estimated area of defect calculated using ImageJ software, after thresholding for 0 and 10cm positioning of the phantom on the imaging table.

0 cm phantom position (mm ²)	10 cm phantom position (mm ²)
33.499	37.327
34.040	37.543
32.894	38.214
33.780	38.495
33.348	38.906

Table 3

Fig 8 and 9 below, are the five selected images that were digitally processed using imageJ software, at the 0 and 10 cm positioning of the phantom, the red color region is the defected area, whereas the white region are the highly perfused area.

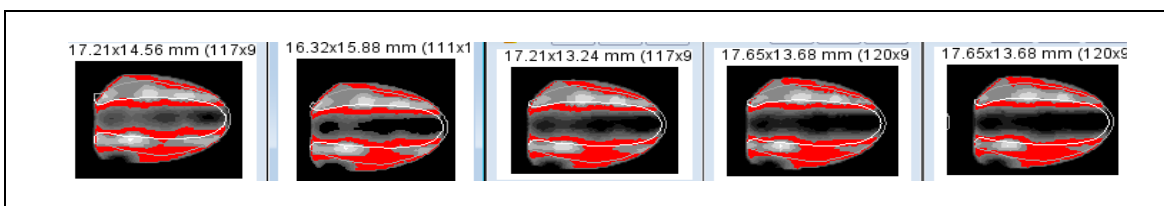


Figure 8: Five selected slices of images at 0 cm position of the phantom, at vertical axis (thresholded)

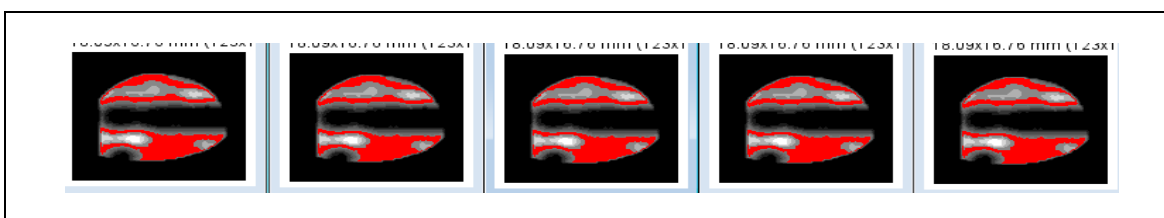


Figure 9: Five selected slices at 10 cm position of the phantom, at vertical axis (thresholded)

Paired Samples Statistics					
		Mean	N	Std. Deviation	Std. Error Mean
Pair 1	mean1	33.51220	5	.435774	.194884
	mean2	38.09700	5	.656961	.293802

Table 4: mean of the 0 and 10 cm positioning of the phantom calculated by SPSS 21

4.3. Discussion

From table 3 above, the estimated area of the MI defects were calculated using imageJ for different positions of the phantom on the table couch and were recorded respectively. Five slices were selected just as in 4.1 above. Comparing the mean estimated area of the two positions, the position of the phantom at 10 cm gives an estimated area closer the actual size of the MI defect, which is about 38.09700 ± 0.65696 in comparison with the 0 cm position of $33.51 \text{ mm}^2 \pm 0.4358$.

The underestimation of the estimated defect area at the 0 cm position could be as a result of attenuation/scatter factors which are dependent on source to collimator face distance. Images obtained with a gamma camera are degraded by the spatially varying collimator–detector response (CDR). For parallel-hole collimators, the CDR depends approximately linearly on the distance from the collimator face. The CDR has geometric, septal penetration and septal scatter components. These correspond, respectively, to photons passing through the collimator holes, photons passing through the septa without interacting, and photons scattering in the septa and resulting in a detected photon. The latter two effects tend to reduce image contrast, can produce star artifacts and introduce distance dependent sensitivity variations, and consequently, attenuate the photon intensity, which may reduce or underestimate the radionuclide distribution in the defected area.

From table 4, SPSS 21 was used to calculate and compare the two means, i.e., mean area for both the thresholded images at 0 and 10 cm position of the phantom on the table, the calculated mean and standard deviation were $33.51 \pm 0.436 \text{ mm}^2$ for and $38.09 \text{ mm}^2 \pm 0.657$. The P-value is < 0.001 , which indicates a strong statistical significant difference between the two means.

5. Conclusion

The results show that accurate quantitation of relative infarct size is possible, with the aid of ImageJ software by thresholding to distinguish an area with a defect from an area without a defect. By thresholding, the defected area was measured which almost approximate the actual size of the defects area. SPECT using a ^{99m}Tc – tagged radioisotope can accurately measure myocardial

defects (MI). Thresholding not only aid in accurate infarcts quantitation, it also increases the signal to noise ratio, which enhances the contrast of the region of interest.

Accurate or optimum positioning of the heart as demonstrated by the phantom study can aid in determining actual infarcts size. This was attributed to the positioning of the phantom on the imaging table. Positioning the phantom far from the collimator face could degrade the image quality due to attenuation and scatter of radiation, which may result in underestimating the estimated infarcts area. Reconstruction algorithm (FBP) used in this study ignores attenuation and scatter correction, which resulted in image degradation and image noise. Radionuclide transmission method used for photon attenuation correction is not ideal, because it gives a disappointing result.

Paired t-test was done using SPSS 21, which indicates a strong statistical significance difference between the raw data and the thresholded data. The estimated mean of the two different positioning of the phantom also shows a statistical significance difference.

6. Limitations on the Phantom Studies

Our study had several limitations. First, phantom images may not closely mimic human myocardial infarctions. The bigger tank which contains the background solution, cannot mimic actual human body, because the internal organs of the human body is made up of different tissues, with different densities, and so will results in different mode of attenuation and scattering of radiation. Secondly, all acquisitions and data points derive from a single phantom source and activity – loading. For clinical application, many additional factors such as motion and patient-induced scatter may complicate corrections and degrade image quality, and in vivo studies are warranted.

7. References

- i. Bruyant, P. P. (2002). Analytic and iterative reconstruction algorithms in SPECT. *Journal of Nuclear Medicine*, 43(10), 1343-1358.
- ii. Chang, L.-T. (1978). A method for attenuation correction in radionuclide computed tomography. *Nuclear Science, IEEE Transactions on*, 25(1), 638-643.
- iii. Cherry, S., Sorenson, J., & Phelps, M. (2003). *Physics in Nuclear Medicine*, ; 2003. Saunders: Philadelphia.
- iv. Cherry, S. R., Sorenson, J. A., & Phelps, M. E. (2012). *Physics in nuclear medicine: Elsevier Health Sciences*.
- v. Collins, T. J. (2007). ImageJ for microscopy. *Biotechniques*, 43(1 Suppl), 25-30.
- vi. DePuey, E. G., & Rozanski, A. (1995). Using gated technetium-99m-sestamibi SPECT to characterize fixed myocardial defects as infarct or artifact. *Journal of nuclear medicine: official publication, Society of Nuclear Medicine*, 36(6), 952-955.
- vii. Doi, K. (2007). Computer-aided diagnosis in medical imaging: historical review, current status and future potential. *Computerized medical imaging and graphics*, 31(4), 198-211.
- viii. Germano, G. (2001). Technical Aspects of Myocardial SPECT Imaging*. *Journal of Nuclear Medicine*, 42(10), 1499-1507.
- ix. Hachamovitch, R., Berman, D. S., Kiat, H., Merz, C. N. B., Cohen, I., Cabico, J. A., . . . Diamond, G. A. (1996). Effective risk stratification using exercise myocardial perfusion SPECT in women: gender-related differences in prognostic nuclear testing. *Journal of the American College of Cardiology*, 28(1), 34-44.
- x. Hartig, S. M. (2013). Basic image analysis and manipulation in ImageJ. *Current protocols in molecular biology*, 14.15. 11-14.15. 12.
- xi. Kundel, H. L., & Revesz, G. (1976). Lesion conspicuity, structured noise, and film reader error. *American Journal of Roentgenology*, 126(6), 1233-1238.
- xii. Lindahl, D., Lanke, J., Lundin, A., Palmer, J., & Edenbrandt, L. (1999). Improved classifications of myocardial bull's-eye scintigrams with computer-based decision support system. *The Journal of Nuclear Medicine*, 40(1), 96.
- xiii. Lusted, L. B. (1960). Logical Analysis in Roentgen Diagnosis: Memorial Fund Lecture 1. *Radiology*, 74(2), 178-193.
- xiv. Lyra, M., & Ploussi, A. (2011). Filtering in SPECT image reconstruction. *Journal of Biomedical Imaging*, 2011, 10.
- xv. Pedersen, J., Steinkuhler, C., Wesser, U., & Rotilio, G. (2011). Rasband, WS, ImageJ, US National Institutes of Health, Bethesda, Maryland, USA.
- xvi. Qi, J., & Leahy, R. M. (2006). Iterative reconstruction techniques in emission computed tomography. *Physics in medicine and biology*, 51(15), R541.
- xvii. Underwood, S., Anagnostopoulos, C., Cerqueira, M., Ell, P., Flint, E., Harbinson, M., . . . Shaw, L. (2004). Myocardial perfusion scintigraphy: the evidence. *European journal of nuclear medicine and molecular imaging*, 31(2), 261-291.
- xviii. Van Laere, K., Koole, M., Lemahieu, I., & Dierckx, R. (2001). Image filtering in single-photon emission computed tomography: principles and applications. *Computerized medical imaging and graphics*, 25(2), 127-133.